https://doi.org/10.5194/nhess-2023-126
Preprint. Discussion started: 14 September 2023

Natural Hazards and Earth System Sciences
Open Access
Discussions

Modelling debris flow runout considering grain size distributions of debris flows at the Illgraben, Swiss Alps

[1,2]Daniel Bolliger, [1]Fritz Schlunegger[*], [3]Brian W. McArdell

[1]Institute of Geological Sciences, University of Bern, Switzerland
[2]Geotest AG, Zollikofen, Switzerland
[3]Swiss Federal Institute WSL, Switzerland
*Corresponding author: fritz.schlunegger@unibe.ch

Abstract

Debris flows are important processes for the assessment of natural hazards due to their damage potential. To assess the impact of a potential debris flow, parameters such as the flow velocity, flow depth, maximum discharge and the volume are of great importance. This study uses data from the Illgraben observation station to explore the relationships between these flow parameters and the debris flow dynamics. The flows were simulated with the RAMMS debris flow runout model, which is based on a numerical solution of the shallow water equations for granular flows using the Voellmy friction relation. Here, the events were modeled in an effort to explore the friction parameters μ and ξ, which describe the basal friction and the viscous turbulent friction, respectively, in the model. Additionally, sediment samples from levee deposits were analyzed for their grain size distributions (14 events) and their mineralogical properties (four events) to explore if the properties of the fine-grained matrix have an influence on the debris flow dynamics. Finally, field data from various debris flows such as the flow velocities and depths were statistically compared with the grain size distributions, the mineralogical properties, and the simulation results to (ii) identify the key variables controlling the kinematics of these flows. The simulation results point to the existence of several ideal solutions, with the friction parameters μ and ξ showing a strong dependency on the Froude number of the flow. It is also shown that no statistically significant correlation exists between the grain size distribution, the mineralogical composition of the matrix, and the debris flow properties, confirming the notion that a fixed debris-flow friction relation or rheology is a limiting assumption, at least for the Voellmy relation. Rather, the flow properties appear to be determined by the flow volume, from which most other parameters can be derived, consistent with common engineering practice.

https://doi.org/10.5194/nhess-2023-126
Preprint. Discussion started: 14 September 2023

Natural Hazards and Earth System Sciences
Open Access
EGU
Discussions

1 Introduction

1.1 Debris flow processes

Debris Flows are rapid mass movements consisting of water-saturated and poorly sorted debris with a larger range of grain sizes. Debris flows tend to develop one single or a suite of multiple surges with steep coarse-grained fronts with low pore fluid pressures, and their motion is driven by gravity and resisted by friction within the flow and at the boundary with the channel bed (Iverson, 1997). The boulder-rich front is then followed by a tapering body where the pore fluid pressures are high, often exceeding the hydrostatic pressure (Iverson, 1997, McArdell et al., 2007). There, larger particles tend to ascend in the debris flow body thereby building a coarse-grained top layer (Johnson et al., 2012). Such aggregation of larger boulders is mainly due to strong buoyancy forces caused by the laminar flow in the front, which results in a grain-size segregation and thus in a shift of the larger particles to the front and the top of the flow. In addition, because this top layer tends to have a larger flow velocity than the debris flow front, the fine-grained material in the surge head is preferentially reincorporated into the body, whereas the coarser-grained particles tend to accumulate in the surge head and are deposited laterally in levees just a few meters behind the front (Johnson et al., 2012).

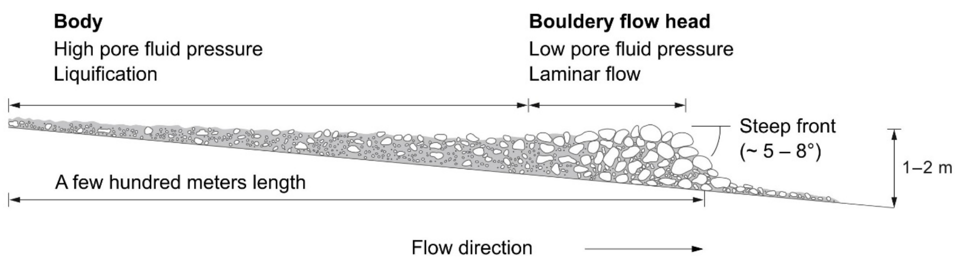

Figure 1: General architecture of a debris flow modified after Pierson (1986).

1.2 Parameters controlling debris flow processes

De Haas et al. (2015) conducted experiments to investigate how the grain size distribution and water content influences the dynamics of a debris flow. They found that a higher clay content tends to result in an increase of both the velocity and the runout distance of such flows. However, if the clay content becomes too large, then the velocity decreases due to a higher viscosity of the fluid. This relationship should also be applicable to the silt fraction because clay and silt particles are a part of the fluid while grains larger than silt contribute to the solids of a debris flow (Iverson, 1997). The experiments of de Haas et al. (2015) also showed that a large gravel content in the flow front leads to a strong frictional resistance, which in turn reduces the flow velocity. In addition, a large gravel content results in a larger pore water diffusivity, which reduces the pore pressure and thus the mobility of the flow. On the

https://doi.org/10.5194/nhess-2023-126
Preprint. Discussion started: 14 September 2023

Natural Hazards and Earth System Sciences
Open Access
Discussions

other hand, a low gravel content leads to lower collisional forces, which might lead to a relatively low flow velocity. Following de Haas et al. (2015), we thus expect a distinct ratio between the clay and gravel contents that allows a flow to reach a maximum velocity. Furthermore, also according to the experiments by de Haas et al. (2015), the water content, the velocity and the runout distance of a debris flow are positively correlated to each other. In addition, these authors demonstrated that a larger volume leads to an increase in the flow velocity. The study of Hürlimann et al. (2015), based on a combination of experimental and field data, suggests a positive correlation between volume, water content and runout distance. They additionally found that an increase in clay content generally leads to a reduction in the runout distance.

1.3 Physical-mathematical models describing debris flow processes

Due to the complexities outlined above, the quantitative process description of debris flows has been a challenge. There are several rheological models or flow resistance relationships describing the behavior of such flows (e.g., Allen, 1997; Rickenmann, 1999; Naef et al., 2006). One commonly used approach is the Voellmy friction relation *(1)* (Voellmy, 1955; Salm, 1993; Christen et al., 2012), which is also implemented in the software RAMMS, a software package to simulate debris flow processes (see next section). In the Voellmy friction equation, the frictional resistance of a flow *S* [Pa] is composed of the sum of two friction terms: (i) A dry Coulomb-type friction term describes the frictional resistance between the debris flow and the channel bed and mainly depends on the flow depth; and (ii) a drag or viscous-turbulent friction term describes the internal frictional resistance, which mainly depends on the dynamic pressure and thus on the velocity of the flow. Both components are characterized by the coefficients μ and ξ, which control the value of the Coulomb-type and the viscous-turbulent friction terms, respectively (Christen et al., 2012). Optionally, cohesion stresses can be included in an extended Voellmy friction equation (Bartelt et al., 2015; Berger et al., 2016). Because this additional cohesion term has rarely been used in engineering practice and is apparently relatively small (Berger et al., 2016), it was neglected herein, and the friction equation takes the following form:

$$S = \mu N + \frac{\rho g v^2}{\xi} \, with \, N = \rho h g \cos(\varphi) \qquad (1)$$

where *S* is the frictional resistance [Pa], *ρ* the density of the debris flow, *h* the flow height (or flow depth), *g* the gravitational acceleration, *φ* the slope angle of the channel bed, and *v* the velocity of the flow.

https://doi.org/10.5194/nhess-2023-126
Preprint. Discussion started: 14 September 2023

A simplified approach to characterize a debris flow is the dimensionless Froude number *(2)*, which describes the ratio between inertial forces and gravitational forces:

$$Fr = \frac{v}{\sqrt{gh}} \qquad (2)$$

where *Fr* is the Froude number, *v* the velocity of the flow, *g* the gravitational acceleration and *h* the flow height (Hübl et al., 2009; Choi et al., 2015).

1.4 Modellling debris flow with RAMMS

As mentioned above, a widely applied tool to simulate debris-flow runout is the RAMMS software, which was developed by the Swiss Federal Institute for Forest, Snow and Landscape Research, WSL (WSL, 2022). RAMMS is based on the two-parameter Voellmy-fluid model (Christen et al., 2012; Bartelt et al. 2015). This approach has been successfully applied to snow avalanches, landslides, and debris flows. A major challenge for modelling is the choice of input friction coefficients. If the simulation cannot be calibrated with data that were collected from a previous well-documented event (Christen et al., 2012; Deubelbeiss & Graf, 2011), the input parameters have to be estimated. Because the model results such as the velocity, the run-out distance, and the flow depth are very sensitive to the friction parameters μ and ξ (Bartelt et al., 2015; Christen et al., 2012), the focus of this work is testing RAMMS with high-accuracy field data, including the grain size of specific flows. This is accomplished for the Illgraben debris flow observation station situated in the Central European Alps (McArdell and Sartori, 2021), because data on the thickness, velocity, and density of the flows have been continuously collected in the past years by the WSL (e.g., de Haas et al., 2022). An additional goal is to explore whether the grain size distribution and the mineralogical composition of the debris flow material have an influence on the flow dynamics, because these parameters have been considered as crucial for the understanding of the flow dynamics (see section 1.2).

2 Study site and setting

The Illgraben catchment, which is the focus of this study, is located in the Valais in western Switzerland (Figure 2). It extends from the summit of the Illhorn (2716 m asl) to the outlet of the Illgraben into the Rhone River (610 m asl). The total area of about 9.5 km^2 consists of the Illbach basin covering 4.9 km^2 and the Illgraben basin, which has a spatial extent of 4.6 km^2 (Figure 2a). This latter sub-catchment has been very active and has generated several debris flows each year (Schlunegger et al., 2009; McArdell and Satori, 2022). The rates of sediment discharge in the Illgraben have been exceptionally high for Alpine standards (Berger et al.,

Natural Hazards and Earth System Sciences
Open Access
EGU
Discussions

2011a). Several studies showed that erosion rates and the numbers and extents of debris flows strongly depend on hydro-climatic parameters such as average annual temperature and precipitation rates (Bennett et al., 2013; Hirschberg et al., 2019; 2021a, b).The highly fractured bedrock (Bumann, 2022), belonging to the Penninic nappe stack (Gabus et al., 2008), consists of massive-bedded limestones, quartzites and Triassic schists with dolobreccia interbeds, which were considered to be the main source of the silt and clay fraction that constitute the matrix of the debris flow deposits (Schlunegger et al., 2009). Based on a petrographic analysis of the debris flow deposits these authors also identified two distinct sediment sources in the Illgraben. The material from these two sources is very well mixed in response to repeated deposition and remobilization of sediment within the catchment (Schlunegger et al., 2009). The sediment cascade is subject to seasonal variations, where smaller debris flows events are associated with net sediment accumulation in the channel, while large flows can entrain sediment up to several times their initial mass along their flow paths (Berger et al., 2010; Berger et al., 2011a, b; Schürch et al., 2011).

Grain size analyses conducted on samples collected from the channel bed and debris flow deposits indicated sand contents of 35-40% and clay contents of < 5% (Hürlimann et al., 2003; Schlunegger et al., 2009; Uchida et al., 2021). In the Rhone valley, an alluvial fan has formed covering an area of 6.6 km^2 (Schürch et al., 2016). The channel on the fan has a U-shaped cross-sectional geometry with a base that is about 5–10 m wide. For the lowermost 2 km, the gradient of the Illgraben channel ranges from about 7% to 18% (measured over a length of 50 m) with a mean of about 8% (Schlunegger et al., 2009). 31 check dams with vertical drops of up to several meters were constructed along the lowermost 4.8 km of the channel to prevent the flows to further incise into the substratum (McArdell et al., 2007; Badoux et al., 2009). A debris flow monitoring station, situated on the lower fan upstream of the confluence with the Rhone River, was installed in 2000 and has been operated by the WSL since then (Hürlimann et al., 2003; Badoux et al., 2009). At the survey site (Figure 2c), measured parameters include frontal velocity, flow depth, bulk density, maximum discharge rate, volumes, and normal and shear force (McArdell et al., 2007). On average 3 to 5 debris flows have been registered by the measuring station every year. They have generally occurred during intense rainstorms between May and October (e.g., McArdell et al., 2007).

https://doi.org/10.5194/nhess-2023-126
Preprint. Discussion started: 14 September 2023

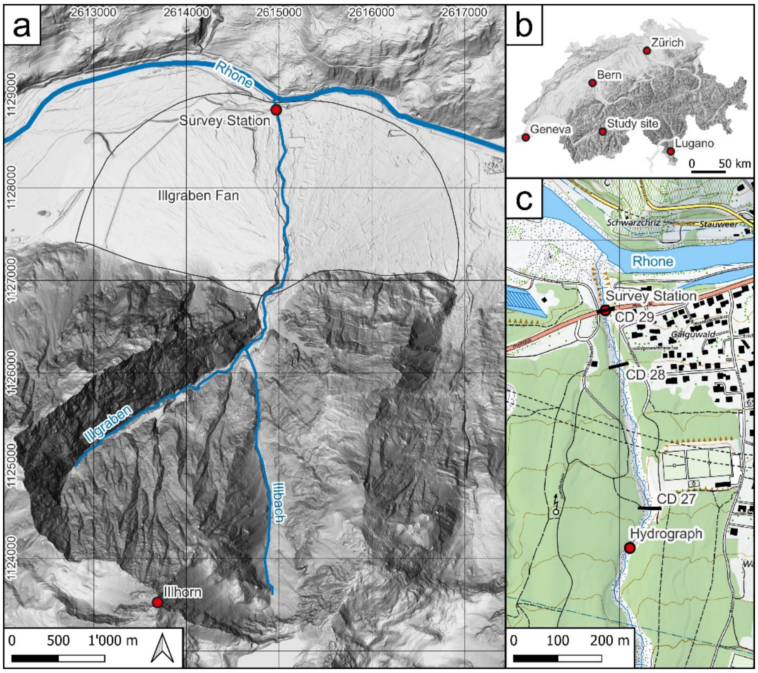

Figure 2: (a) Overview of the topographic situation around the Illgraben showing the Illgraben system with its river network consisting of the Illgraben, Illbach and the Rhone River. (b) Overview map of Switzerland with location of the study site. (c) Detailed topographic map of the Illgraben reach along which the RAMMS simulations have been conducted. It shows the location of the hydrograph which was used as starting position for the modelling. In addition, the three check dams (CD) and the location of the survey station below the Pfynstrasse are displayed on this figure. The background is provided by the swissALTI3D and the Swiss Map Raster 10 (Swisstopo, 2022).

3 Methods

Because the flow properties depend on the values of the friction parameters μ and ξ, we conducted simulations with the RAMMS software and iteratively changed the μ and ξ coefficients until we found, for each event, a best fit between the simulation results and the observations. These simulations will allowed us to identify those pairs of friction parameters that best explain the measured conditions of the simulated flows (such as the flow velocity and the flow depth). We then tested the dependency of the input parameters on the measured debris flow properties using statistical methods and the software Matlab (R2021b). Because we hypothesize that the grain size distribution of the fine-grained fraction, and possibly the mineralogical composition of the debris flows, influence the friction of the flow, we finally tested these relationships using grain size and XRD data collected from the flow deposits.

3.1 Numerical modelling with RAMMS

The use of RAMMS requires a digital elevation model (DEM), event volume and peak discharge. The drone-based DEM, which is based on a survey conducted on the 10th of August 2021 (de Haas et al., 2022), was used for all simulations. However, this high-resolution DEM

https://doi.org/10.5194/nhess-2023-126
Preprint. Discussion started: 14 September 2023

did not cover the section of the channel between the Pfynstrasse and the Rhone River (Figure 2c). Therefore, in order to extend the area towards the confluence with the Rhone, the photogrammetry DEM was combined with an existing 0.5 m-lidar DEM (Swisstopo, 2022) using the software QGIS. The DEM of the short, concrete channel section beneath the road bridge had to be reconstructed manually since it was not possible to image the topography below the bridge. In addition, a filter (Serval-Raster editing tools, version 3.10.2) was applied to the channel bed to smoothen the bed surface. This was done because a large local change in topography (such as a boulder) can induce strong vertical accelerations in RAMMS, which can lead to unrealistically large (or small) local flow depths.

We employed the 'hydrograph' input option of RAMMS to model the flows, which releases a completely developed debris flow with user-specified velocity, volume, density, and time-dependent discharge values. The hydrograph input was placed upstream of the football field c. 500 m upstream of the survey site (check dam 27, Figure 2c). Erosion was allowed to occur along the entire channel (Frank et al., 2015; 2017), but not at the check dams. The friction parameters μ and ξ were systematically adjusted for each event until a best fit was reached between the modelled and observed flow velocities v and flow depths h. Similar to the survey in the field, the model velocity was calculated using the travel time between check dams 28 and 29 (Figure 2c). The flow depth values were obtained as the average of the measurements that were conducted at four points along a cross section at check dam 29. Finally, in order to test the representativeness of a simulation, we introduced a dimensionless z-value *(3)*, which we used to describe the deviation of the simulated velocity v and flow depth h from the real measurements:

$$z = \sqrt{\left(\frac{v_{simulation} - v_{measured}}{v_{measured}}\right)^2 + \left(\frac{h_{simulation} - h_{measured}}{h_{measured}}\right)^2} \qquad (3).$$

The friction coefficient μ is sometimes expressed as the tangent of the internal shear angle (WSL, 2022). According to Salm (1993) an internal movement parallel to the slope is only possible if the internal shear angle is smaller than the slope angle. Consequently, the value of μ should be smaller than the tangent of the channel slope angle. For a minimum slope angle of 7%, which is equivalent to 4°, μ should thus be smaller than 0.07. Therefore, for every debris flow event, we conducted several simulations with μ varying from 0.01 to 0.06, and we modified the ξ parameter to minimize the z-value. This resulted in μ–ξ pairs with lowest z-values and thus best fits between model results and observations.

3.2 Grain size distribution

For most of the debris flows that occurred in the years 2019, 2021 and 2022, at least one sediment sample of 1.5 to 3 kg was taken from the levee deposits under the bridge (Swiss coordinates: 2'614'973, 1'128'842; Figure 2c) to prevent effects related erosion and dilution by rainfall. The levees were chosen because they are considered to record the grain size composition of the surge head, which in turn has the potential to determine the dynamics of the debris flow (Johnson et al., 2012). The samples were processed using state-of-the-art methods (SN670 004–2b–NA norm) at the Bern University of Applied Sciences (Burgdorf). Accordingly, the material was dried and sieved to a minimum particle size of 0.5 mm using a defined set of mesh sizes. Subsequently, a slurry test was carried out on the material < 0.5 mm using a hydrometer. The goal of this task was to determine the particle size distribution between 0.1 and 0.001 mm. Finally, the grain size distribution between 0.5 and 0.063 mm was determined by wet sieving. The grain size distribution was truncated at 16 mm so that the entire sample is at least 100 times the mass of the largest particle (e.g., Church et al., 1987).

3.3 Powder XRD

We infer that clay minerals influences the pore pressure of the flow (Barshad, 1952), which in turn could influence its mobility (McArdell et al., 2007). To test this hypothesis, the mineralogical properties of some debris flow samples were measured through standard powder XRD diffraction at the Institute of Geological Sciences of University of Bern. For this purpose, four samples were chosen from fast and slow velocity flows as well as from deposits where either the coarse-grained or the fine-grained fractions dominate. To this end, the grain size fraction < 0.063 mm, which was already extracted during the steps outlined above, was analyzed for powder XRD diffraction. Subsequent milling with a vibrating disc mill (Retsch RS 200) and a McCrone XRD-mill reduced the particle sizes to the sub-micrometer scale. Corundum powder was added as standard to the samples, and the samples were measured with the x-ray diffractometer X'Pert Pro MPD with Cu radiation. Because this step did not include a determination of the mineralogic composition of the clay minerals, a slightly different approach had to be employed to identify the nature and composition of the clay minerals. Here, we used the same initial material, but it was only milled with the vibrating disc mill. The powder was then mixed with a dispersant (0.1 molar NH_3) to achieve a homogeneous suspension. The clay particles were separated in an Atterberg cylinder. The particles still in suspension after 15 hours were extracted using a centrifuge. The extracted clay particles were then cleaned with HCl, $CaCl_2$ and deionized water. To distinguish between the different clay minerals, three sample holders were either air dried, treated with ethylene glycol or heated to 400°C and 550°C before measuring with the X'Pert Pro MPD with Cu radiation. The final

https://doi.org/10.5194/nhess-2023-126
Preprint. Discussion started: 14 September 2023

processing of the data was carried out with the software TOPAS (Coelho, 2018), which uses a Rietveld structure refinement technique (Rietveld, 1969).

4 Results

4.1 Survey results

A total of 13 events from 2019, 2021, and 2022 were analyzed (Appendix A, Table 1). The measured flow velocities vary by one order of magnitude from 0.89 m/s to 8.69 m/s. The maximum flow depths range from 1.13 m to 3.13 m. Accordingly, the Froude numbers range from 0.27 to 2.35, pointing towards considerable differences in the dynamics of these flows. The total volumes reach a maximum of c. 176.000 m^3 and the maximum discharge rates were c. 190 m^3/s. The measured density ranges from 1189 kg/m^3 to 2323 kg/m^3, and the related volumetric water contents were between c. 20% and 90%.

Table 1: Measured and analyzed debris flow events from 2019, 2021, and 2022. Velocity, flow depth, volume, maximum discharge (Qmax) and density are the results of direct measurements at monitoring station in the Illgraben. The Froude number was derived from these. The last two columns show, for which events XRD analyses and RAMMS simulations were performed. The event of the 26th of July 2019 could not be simulated due to the high Froude number.

Event date	Velocity [m/s]	Flow depth [m]	Froude number [ ]	Volume [m^3]	Qmax [m^3/s]	Density [kg/m^3]	XRD analysis	RAMMS simulation
21.06.2019	6.62	3.13	1.19	97394	147.61	1870		✓
02.07.2019	3.86	1.75	0.93	73188	65.58	1971	✓	✓
26.07.2019	8.69	1.39	2.35	113310	93.26	2223	✓	
11.08.2019	6.95	1.81	1.65	88064	95.63	2323		✓
20.08.2019	0.89	1.13	0.27	6137	8.06	2031	✓	✓
24.06.2021	8.18	2.40	1.69	105032	162.20	1750		✓
06.07.2021	8.69	2.50	1.75	76906	186.61	1605		✓
16.07.2021	2.78	2.38	0.58	80879	60.70	1916	✓	✓
07.08.2021	2.32	2.49	0.47	38737	41.19	1884		✓
19.09.2021	1.25	1.13	0.38	8538	10.67	1697		✓
05.06.2022	3.39	2.08	0.75	39498	55.42	1690		✓
04.07.2022	8.18	2.49	1.66	175929	169.14	1189		✓
08.09.2022	1.91	1.93	0.44	9283	20.94	1592		✓

4.2 Numerical modelling with RAMMS

Because the main output parameters from the RAMMS simulations (Appendix B) were velocity and flow depth (Figure 3), the Froude number (eq. 2) proved to be useful for characterizing these flows. Please note that in this context equation *(2)* predicts that changes in the flow velocity have a larger impact on the Froude number than variations in flow depth. The simulations showed that RAMMS produces reasonable results for Froude numbers up to about 1.75. For larger values (e.g., flows with large flow velocities), the simulations predict the occurrence of standing waves, which have not been observed during this study. Flows with

https://doi.org/10.5194/nhess-2023-126
Preprint. Discussion started: 14 September 2023

large Froude numbers tend to be characterized by roll-waves, which may correspond to the predicted standing waves by RAMMS. Therefore, no simulations were possible for the event on the 26th of July 2019, because this flow was characterized by a Froude number of 2.35. Also, the occurrence of roll-waves, which could be observed in some real debris flows, could not be modeled with RAMMS.

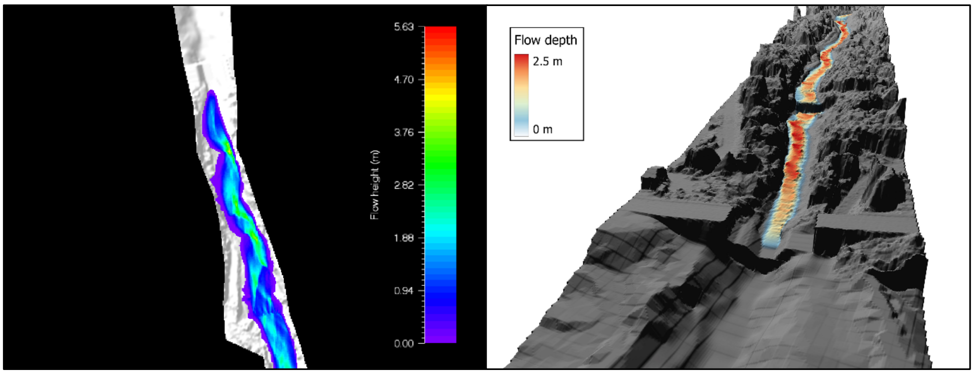

Figure 3: Example of simulated flow depths. The image on the left shows flow depths in a 2D view provided by the RAMMS software. The image on the right shows a 3D view of the debris flow projected on a hillshade model using the QGIS software.

The model results show that more than one best-fit μ–ξ pair is possible. The μ–ξ pair with μ = 0.01 has, on average, the lowest *z*-value, followed by the pairs with μ = 0.02 and μ = 0.05. These relationships also show a strong dependency on the corresponding Froude numbers (Figure 4).

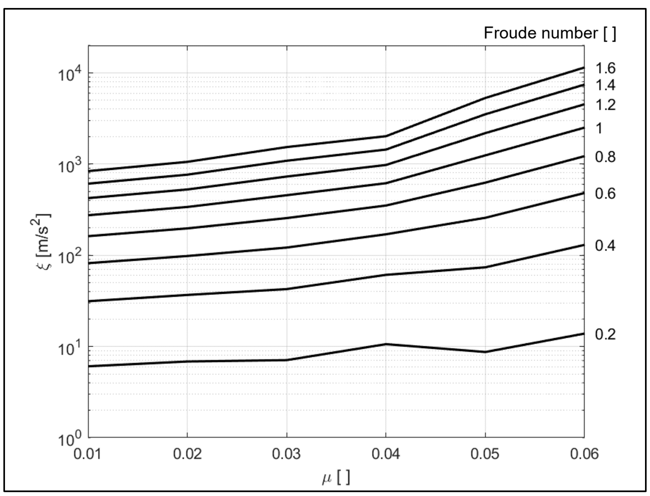

Figure 4: Ideal μ–ξ pairs, which result in a best fit between the observed and the modelled debris flow parameters, which, in turn, appear to depend on the Froude numbers of the corresponding debris flow events.

https://doi.org/10.5194/nhess-2023-126
Preprint. Discussion started: 14 September 2023

The total friction *S* is the sum of a basal friction component that is scaled by *μ,* and an internal friction contribution, which in turn depends on *ξ* (see above). Figure 5 shows the absolute values of the friction components as a function of the selected *μ*-value. Debris flows dominated by basal friction (large *μ*) tend to appear more turbulent on the video recordings. Because we found ideal *μ*–*ξ* pairs with *μ* = 0.01–0.02 and *μ* = 0.05 for most debris flows, we considered these flows to be dominated either by (i) the internal friction (flows with *μ* = 0.01–0.02) and thus less turbulent, hereafter termed ‘laminar’, or by (ii) the basal friction (flows with *μ* = 0.05), hereafter termed ‘turbulent’. Note that Figure 5 also shows that the total friction *S* increases with a larger *μ*. Nevertheless, the output of the simulation (velocity and flow depth) is similar regardless of which *μ*–*ξ* pair variant is chosen.

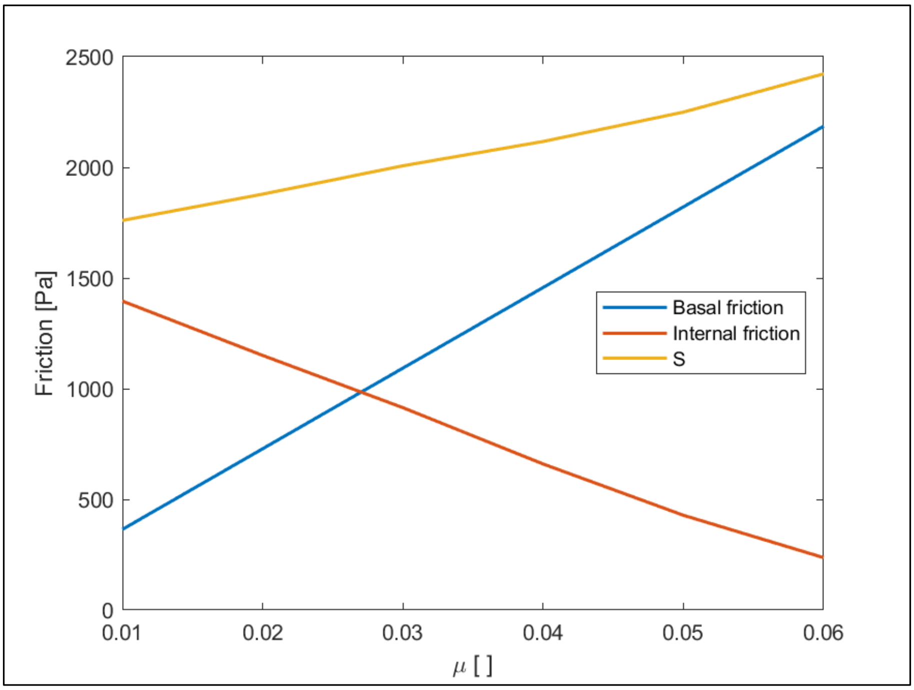

Figure 5: Values of basal friction, internal friction, and total friction *S* as a function of the selected Coulomb friction coefficient *μ*. The plotted values are averages of the friction magnitudes of all best-fit simulations.

4.3 Grain size distribution

Samples from 14 debris flows were analyzed for their grain size distribution (Figure 6 and Appendix C). Note that there was a sediment sample but no monitoring data for the event on the 4th of October 2021. All events show a very similar grain size distribution. An exception, and thus an outlier, is a sediment sample that has a larger relative abundance of fine-grained material. This sample was taken from a debris flow, which occurred on the 2nd of July 2019.

https://doi.org/10.5194/nhess-2023-126
Preprint. Discussion started: 14 September 2023

The clay fraction has a relative mass abundance of 2–3%, the silt fraction 27–35%, the sand fraction 27–40% and the part of the gravel fraction that is covered by the analysis 23–37%. Note that the gravel fraction was just recorded up to a grain size of 16 mm, because it was not feasible to collect larger mass-representative samples. We measured grain sizes of 0.015–0.02 mm for the 16% percentile, 4–9 mm for the 84% percentile and 10–15 mm for the 95% percentile. The median grain size ranges from 0.15 mm to 0.5 mm. In general, the material was very poorly sorted with a skewness towards the fine-grained fraction.

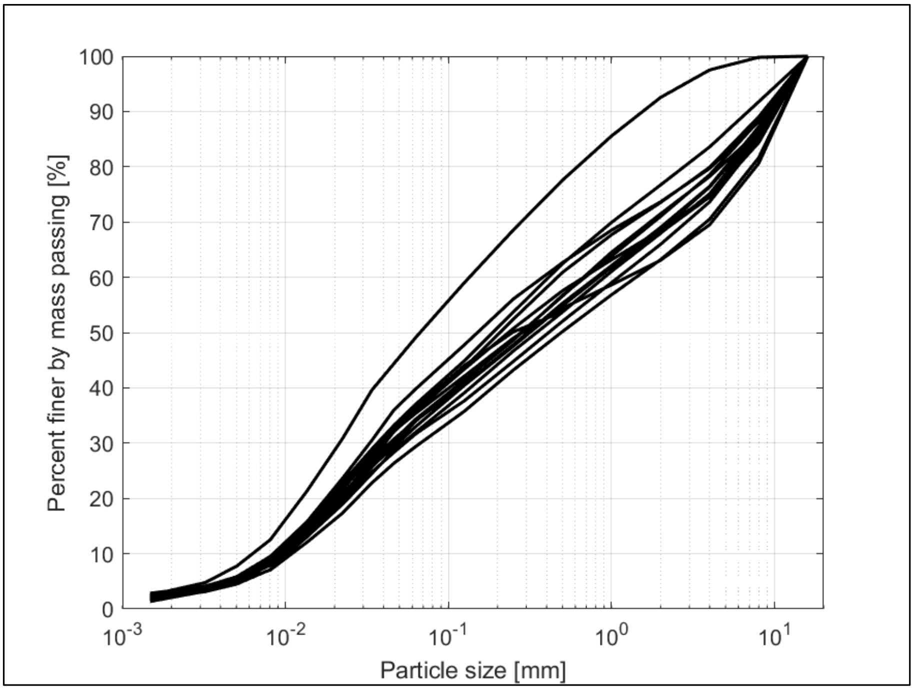

Figure 6: Diagram showing the grain size distribution of all 14 sampled debris flow deposits, calibrated to a maximum grain size of 16 mm.

4.4 Powder XRD

The results of the powder XRD analysis (Appendix D) show that quartz was the main mineral of the silt fraction and contributes between 29 and 36 wt% (Figure 7). In addition, dolomite (17–24 wt%), muscovite (18–22 wt%), calcite (7–18 wt%) and illite minerals (8–12 wt%) are present in all samples. Feldspar grains occur by < 5 wt%, and the clay minerals chlorite, kaolinite and smectite are measured in small quantities (< 1%) or are below the detection limit. Calcite shows the greatest variation in the mineralogical composition with differences up to 11 wt%. The other main components quartz, dolomite, muscovite and illite show variations with a maximum of 7 wt%. The feldspar minerals albite and orthoclase are very homogeneously

https://doi.org/10.5194/nhess-2023-126
Preprint. Discussion started: 14 September 2023

distributed in the four samples. Overall, the variations in the mineralogical composition between the different samples are only minor and often lie within the methodological error of ± 10% of the measured values.

From the clay minerals, only smectite can absorb larger amounts of water (Likos & Lu, 2002). However, the x-ray spectra of muscovite and smectite cannot be distinguished with the applied XRD method. Because the Triassic schists are considered to be the source of the clay minerals in the catchment area (Schlunegger et al., 2009), the signal is more likely related to fine-grained muscovite (sericite) than to smectite minerals. Therefore, swelling clay minerals are expected to be of minor importance in this case.

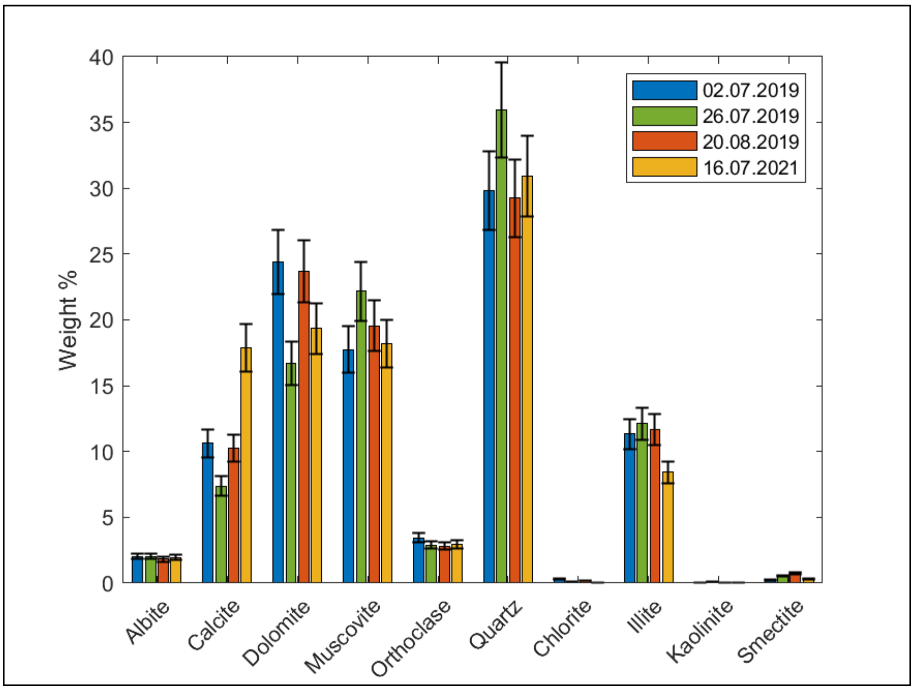

Figure 7: Mineralogic composition of four samples analyzed by powder-XRD. The black error bars indicate a methodological error of 10% of the measured value. The material representing the flow on the 2nd of July 2019 was exceptionally fine-grained; the flow on the 26th of July of the same year was an event with a high velocity (8.69 m/s). The debris flows on the 20th of August, again in 2019, was very slow (0.89 m/s), and that on the 1st of August 2021 was characterized by a rather coarse-grained matrix.

4.5 Statistical evaluation of the debris flow properties

A statistical evaluation of the parameters of the debris flows measured at the monitoring station shows a positive correlation between velocity, flow depth, volume, and maximum discharge (Figure 8). While velocity, volume, and maximum discharge correlate very strongly among themselves as they are physically related (auto-correlation), the correlation of these parameters with the flow depth is less evident, yet a weak positive correlation is certainly

https://doi.org/10.5194/nhess-2023-126
Preprint. Discussion started: 14 September 2023

Natural Hazards and Earth System Sciences
Discussions

visible. As expected, the values of the Froude number correlate positively and strongly with the velocity (auto-correlation) and also positively with the volume and the maximum discharge of the flows. No correlation can be found between the Froude number values and the flow depths, which illustrates the dominance of the velocity on the Froude number in our case. If just the volume of the sediment load is considered, the correlations become less strong for most of the parameters. Yet, positive correlations between this variable and the flow velocity, and especially with the Froude number, are apparent. Interestingly, correlations between grain size, clay content and flow properties are not apparent in our analyses (Figure 9).

In summary, a debris flow with a large volume tends to have a large flow velocity and flow depth, which consequently also results in a large maximum discharge and a large Froude number. On the other hand, debris flows that have a small volume are also slow, and they have both a small flow depth and a low Froude number. In addition, no correlation between the inferred water content and the volume or maximum discharge was found for these events. Yet, the total friction values that are extracted from the modelling results show a clear positive correlation with the flow depth, and a weak positive correlation with the density and thus the water content (Figure 9).

https://doi.org/10.5194/nhess-2023-126
Preprint. Discussion started: 14 September 2023

Natural Hazards and Earth System Sciences
Open Access
Discussions

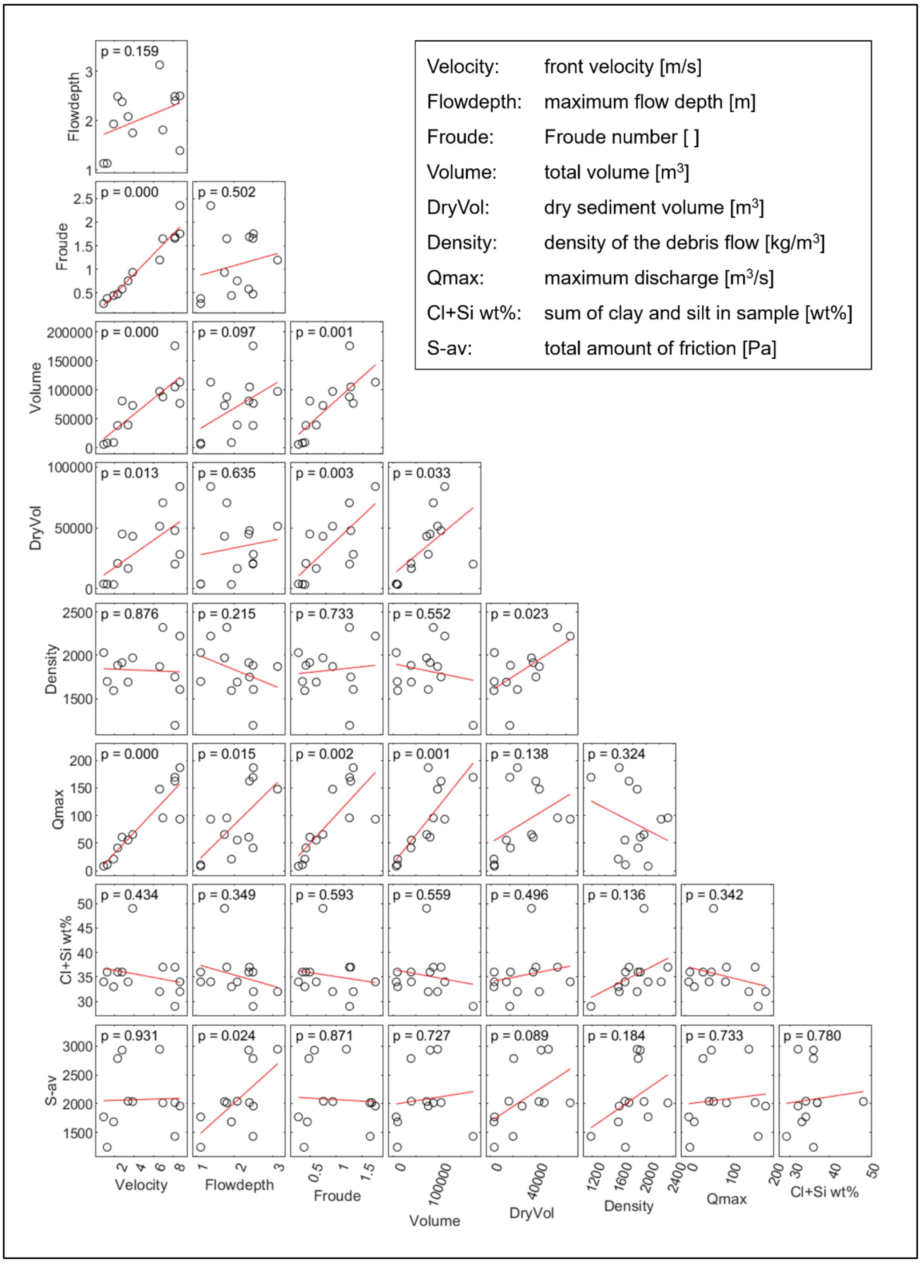

Figure 8: Statistical correlations between dynamic properties of the debris flows with a statistical p-value. For correlation tests a significance level of 0.05 is considered. Correlations with p-values8 < 0.05 can therefore be considered as significant. Measurements from the monitoring station at the Illgraben and values derived from them are front velocity [m/s], maximum flow depth [m], Froude number [ ], total volume [m^3], dry sediment volume [m^3], density of a flow [kg/m^3], which points to the water content and the maximum discharge [m^3/s]. From the grain size analyses, we have the percentage of the sum of clay and silt in the sample [wt%]. From the modeling with RAMMS we get the total amount of friction [Pa] as average of all best-fit simulations of a certain event. The plots were accomplished using a modified version of the Correlation Matrix Scatterplot by Chow (2022) designed for MATLAB. Note that a statistical p-value with p = 0.000 means that the value is less than 0.0005, and therefore it is rounded down to 0.

https://doi.org/10.5194/nhess-2023-126
Preprint. Discussion started: 14 September 2023

Natural Hazards and Earth System Sciences
Discussions

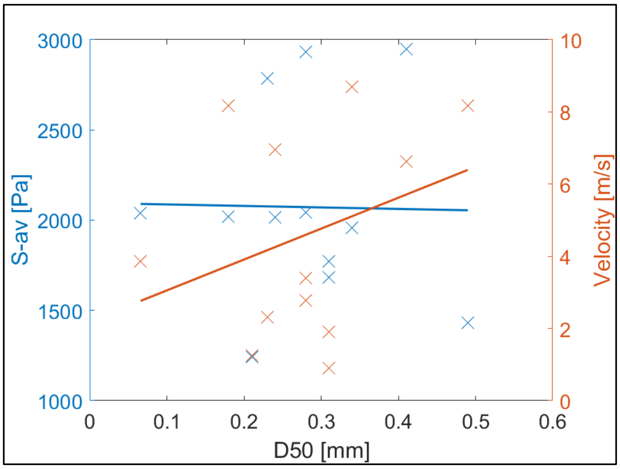

Figure 9: Correlation (first order polynomial trendlines accomplished by least square fitting) between the total amount of friction S-av as average of all best-fit simulations of a certain event and the D50 value of the corresponding sediment sample (blue), and correlation between the measured velocity of the flow and the D50 value of the corresponding sediment sample (red).

5 Discussion

The registered debris flows in the years 2019, 2021 and 2022 show large differences in their dynamics, where flow depths and flow velocities varied by a factor of 3 and even 10, respectively. Despite these variabilities in the surveyed parameters, most of the flows could be simulated with RAMMS, and the model outputs yielded consistent results regarding the underlying controls and the simulated flow kinematics and properties. In the following section, we discuss how the various parameters such as the grain size and mineralogical distribution of the fined-grained matrix as well as the friction properties potentially exerted a control on the surveyed debris flows.

5.1 Relationships between volume, flow velocity and flow depth, and controls on friction properties

The statistical tests show positive correlations between volume, flow velocity, flow depth and maximum discharge rate. Our results are thus consistent with similar results reported by Rickenmann (1999), de Haas et al. (2015) and Hürlimann et al. (2015). Indeed, flows with larger volumes probably contain a larger number of pebbles and boulders, which according to Johnson et al. (2012) are likely to accumulate on the front of these flows. As a result, the frictional resistance of the frontal part increases (Iverson, 1997), with the consequence of a damming effect such as that the flow depths will increase. We indeed see such mechanisms at work in the surveyed flows through positive correlations between flow depth, flow velocity and flow volume. We thus infer that the volume can be considered as the most important driving parameter for explaining the debris flow dynamics in the Illgraben system and therefore

Natural Hazards and Earth System Sciences
Discussions

can be considered as a key parameter. This confirms standard practice in hazard analysis, which gives primary importance to event volume.

The evaluation of the RAMMS simulations shows that there are several solutions to reliably simulate a given event with known properties. In detail, the flows can be interpretated as dominated by basal friction (large Voellmy μ values) or dominated by internal friction (low Voellmy ξ values, which yields a large internal friction according to equation *1*). We speculate that which of these two solutions is more accurate for a given event could possibly be determined by measuring the internal distribution of the flow velocities. Large and variable internal flow velocities could be attributed to occurrence of turbulence, which would thus be consistent with a low internal friction, but a large basal friction. Alternatively, a flow with a more homogeneous distribution of internal velocities is more likely to indicate the occurrence of less turbulent (or possibly laminar) flow where viscous shear forces and thus a high internal friction dominate the flow friction (e.g., Figure 5).

5.2 Influence of the grain size distribution and mineralogy

The granulometric analysis of the levee deposits indicates a rather homogeneous grain size distribution for the clay, silt, sand and the fine-grained gravel fraction. The grain size distribution fits quite well with the granulometric analyses of the debris flow deposits at the Illgraben published by Hürlimann et al. (2003). Because of a lack of correlations between the relative proportion of the fine fraction to the parameters that characterize the flow properties (e.g., friction and flow velocity; Figure 9), the variations in the dynamics of these flows cannot be simply explained by a simple fixed friction relation such as the Voellmy relation. This inference is consistent with the notion by Iverson (2003) who states that the evolution of debris flow behavior upstream of the front is likely to be complex. In the same sense, because of the homogeneity of the samples with respect to the grain size distribution of the components smaller than 16 mm, also the relative abundance of the sand and even the fine-grained gravel fraction cannot be related to variations in the flow dynamics. Nevertheless, an influence of the grain size composition on the debris flow dynamics, as described by de Haas et al. (2015) and Hürlimann et al. (2015), cannot be fully excluded. Because the relative abundances of the different fractions are similar, their potential influence on the flow properties should also be similar for each event. Due to this similarity, such relationships (if present) would not be detectable with the measurements presented herein. Admittedly, we also have no information to exclude a potential control exerted by the coarse-grained fraction such as coarse gravel, cobbles, and boulders, on the flow dynamics, as described by de Haas et al. (2015). Attempts to reconstruct the full grain size distribution are hampered by a lack of information on the grain size below the surface of the flow (e.g., Uchida et al., 2021). In addition, the influence of small

https://doi.org/10.5194/nhess-2023-126
Preprint. Discussion started: 14 September 2023

Natural Hazards and Earth System Sciences
Open Access
Discussions

changes of the topography on the results was not investigated here, but could improve the correlations of the flow properties to grain size if adequately considered.

Similar to the grain size distribution of the fine-grained matrix, we do not see a relationship between the mineralogical composition of the matrix and the flow properties. However, the homogeneity in terms of the mineral composition and also the grain size composition between the samples confirms the results of previous studies that inferred the occurrence of an efficient mixing mechanism in the Illgraben (Schlunegger et al., 2009; Berger et al., 2011a).

Conclusion

The results obtained in the Illgraben system by comparing various debris flow parameters with data from runout modelling, grain size analyses, XRD analyses can be summarized as follows:

1) The simulation of debris flows with RAMMS yields multiple solutions with different friction ratios, all of which lead to quite similar results. The coefficients μ and ξ, which are responsible for the scaling of the friction terms in the Voellmy equation, can be estimated from the Froude number of the debris flow.
2) The dynamics of a debris flow in the Illgraben is strongly dependent on its volume. If information about the sediment volume in the source area is available, the parameters for simulating a potentially worst-case debris flow and its impact can theoretically be assessed with some uncertainties.
3) Due to the relatively large homogeneity of the deposits with respect to the grain size distribution and the mineralogical composition, an efficient mixing process in the Illgraben can be inferred.
4) Based on these data, variations in the dynamics of different debris flows cannot be attributed to the grain size distributions of the clay, silt, sand or fine-grained gravel fractions. Consequently, an assessment of a potential debris flow or a definition of a simulation based on grain size compositions in the source area is not adequate in the case presented here.

Such relationships are particularly useful for the assessment of natural hazards, as they provide specific evidence for the estimation of a debris flow and its impact.

Acknowledgement

We are grateful for the technical support provided by Franziska Nyffenegger (grain size analysis), Pierre Lanari and Michael Schwenk (statistics) as well as Frank Gfeller and Anulekha Prasad (XRD analysis). We thank the WSL staff for their support with sampling.

Data availability

All data used in this paper are listed in Table 1 and in the supplementary files.

Autor contributions

FS and BM designed the study. DB conducted the experiments, collected the data and processed the samples. DB wrote the paper, with contributions by FS and BM. All authors discussed the article.

Competing interests

The authors declare that they have no conflict of interest.

References

Allen, P. A.: Earth surface processes. Blackwell Science, 1997.

Badoux, A., Graf, C., Rhyner, J., Kuntner, R., and McArdell, B. W.: A debris-flow alarm system for the Alpine Illgraben catchment: Design and performance, Nat. Hazards, 49, 517–539, 2007. https://doi.org/10.1007/S11069-008-9303-X/FIGURES/7

Barshad, I.: Absorptive and swelling properties of clay-water system, Clays Clay Miner., 1(1), 70–77, 1952.

Bartelt, P., Valero, C. V., Feistl, T., Christen, M., Bühler, Y., and Buser, O.: Modelling cohesion in snow avalanche flow, J. Glaciol., 61, 837–850, 2015. https://doi.org/10.3189/2015JoG14J126

Belli, G., Walter, F., McArdell, B., Gheri, D., and Marchetti, E.: Infrasonic and Seismic Analysis of Debris-Flow Events at Illgraben (Switzerland): Relating Signal Features to Flow Parameters and to the Seismo-Acoustic Source Mechanism, J. Geophys. Res. Earth, 127, e2021JF006576, 2022. https://doi.org/10.1029/2021JF006576

Bennett, G. L., Molnar, P., McArdell, B. W., Schlunegger, F., and Burlando, P.: Patterns and controls of sediment production, transfer and yield in the Illgraben, Geomorphology, 188, 68–82, 2013. https://doi.org/10.1016/j.geomorph.2012.11.029

Berger, C., Christen, M., Speerli, J., Lauber, G., Ulrich, M., And McArdell, B. W.: A comparison of physical and computer-based debris flow modelling of a deflection structure at Illgraben, Switzerland, Data Acquisition and Modelling (Monitoring, Processes, Technologies, Models), 212–220, 2016.

Berger, C., McArdell, B. W., Fritschi, B., and Schlunegger, F.: A novel method for measuring the timing of bed erosion during debris flows and floods, Water Res. Res., 46, 2010. https://doi.org/10.1029/2009WR007993

https://doi.org/10.5194/nhess-2023-126
Preprint. Discussion started: 14 September 2023

Berger, C., McArdell, B. W., & Schlunegger, F.: Sediment transfer patterns at the Illgraben catchment, Switzerland: Implications for the time scales of debris flow activities, Geomorphology, 125, 2011a. 421–432. https://doi.org/10.1016/j.geomorph.2010.10.019

Berger, C., McArdell, B. W., and Schlunegger, F.: Direct measurement of channel erosion by debris flows, Illgraben, Switzerland, J. Geophys. Res., 116, 2011b. https://doi.org/10.1029/2010JF001722

Bumann, N.: Effect of Geological Preconditioning on Sediment Production in the Illgraben Catchment [Ms thesis]. University of Bern, 2022.

Choi, C. E., Ng, C. W. W., Au-Yeung, S. C. H., and Goodwin, G. R.: Froude characteristics of both dense granular and water flows in flume modelling, Landslides, 12, 1197–1206, 2015. https://doi.org/10.1007/S10346-015-0628-8/FIGURES/11

Chow, J. : Correlation Matrix Scatterplot, 2022. https://www.mathworks.com/matlabcentral/fileexchange/53043-correlation-matrix-scatterplot

Christen, M., Bühler, Y., Bartelt, P., Leine, R., Glover, J., Schweizer, A., Graf, C., Mcardell, B. W., Gerber, W., Deubelbeiss, Y., Feistl, T., and Volkwein, A.: Integral hazard management using a unified software environment numerical simulation tool “RAMMS” for gravitational natural hazards, 2012. www.interpraevent.at

Church, M., McLean, D., and Wolcott, J.: River bed gravels : sampling and analysis, Sediment Transport in Gravel-Bed Rivers, 43–88, 1987. https://cir.nii.ac.jp/crid/1572261549037050368.bib?lang=en

Coelho, A. A.: TOPAS and TOPAS-Academic: An optimization program integrating computer algebra and crystallographic objects written in C++, J. Applied Crystall., 51, 210–218, 2018. https://doi.org/10.1107/S1600576718000183

de Haas, T., Braat, L., Leuven, J. R. F. W., Lokhorst, I. R., and Kleinhans, M. G.: Effects of debris flow composition on runout, depositional mechanisms, and deposit morphology in laboratory experiments, J. Geophys. Res. Earth Surface, 120, 1949–1972, 2015. https://doi.org/10.1002/2015JF003525

de Haas, T., McArdell, B. W., Nijland, W., Åberg, A. S., Hirschberg, J., and Huguenin, P.: Flow and Bed Conditions Jointly Control Debris-Flow Erosion and Bulking. Geophys. Res. Lett., 49, e2021GL097611, 2022. https://doi.org/10.1029/2021GL097611

Deubelbeiss, Y., and Graf, C.: Two different starting conditions in numerical debris-flow models - Case study at Dorfbach, Randa (Valais, Switzerland). Jahrestagung Der Schweizerischen Geomorphologischen Gesellschaft, 2011.

Frank, F., McArdell, B. W., Huggel, C., and Vieli, A.: The importance of entrainment and bulking on debris flow runout modeling: examples from the Swiss Alps, Nat. Hazards Earth Sys. Sci., 15, 2569-2583, 2015, https://doi.org/10.5194/nhess-15-2569-2015;

Frank, F., McArdell, B. W., Oggier, N., Baer, P., Christen, M., and Vieli, A.: Debris-flow modeling at Meretschibach and Bondasca catchments, Switzerland: sensitivity testing of field-data-based entrainment model, Nat. Hazards Earth Sys. Sci., 17, 801-815, 2017. https://doi.org/10.5194/nhess-17-801-2017

Gabus, J. H., Weidmann, M., Sartori, M., and Burri M.: Blatt 1287 Sierrre - Geologischer Atlas der Schweiz 1:25 000, Erläuterungen, Bundesamt für Landestopografie swisstopo, 2008.

Hirschberg, J., Badoux, A., McArdell, B. W., Leonarduzzi, E., and Molnar, P.: Evaluating methods for debris-flow prediction based on rainfall in an Alpine catchment, Nat. Hazards Earth Sys. Sci., 21, 2773–2789, 2021. https://doi.org/10.5194/NHESS-21-2773-2021

Hirschberg, J., Fatichi, S., Bennett, G. L., McArdell, B. W., Peleg, N., Lane, S. N., Schlunegger, F., and Molnar, P.: Climate Change Impacts on Sediment Yield and Debris-Flow Activity in an Alpine Catchment, J. Geophys. Res. Earth Surface, 126, e2020JF005739, 2021. https://doi.org/10.1029/2020JF005739

Hirschberg, J., McArdell, B. W., Badoux, A., and Molnar, P.: Analysis of rainfall and runoff for debris flows at the Illgraben catchment, Switzerland. Debris-Flow Hazards Mitigation: Mechanics, Monitoring, Modeling, and Assessment - Proceedings of the 7th International Conference on Debris-Flow Hazards Mitigation, 693–700, 2019.

Hübl, J., Suda, J., Proske, D., Kaitna, R., and Scheidl, C.: Debris Flow Impact Estimation, International Symposium on Water Management and Hydraulic Engineering, 137–148, 2009. https://www.researchgate.net/publication/258550978

Hürlimann, M., McArdell, B. W., and Rickli, C.: Field and laboratory analysis of the runout characteristics of hillslope debris flows in Switzerland, Geomorphology, 232, 20–32, 2015. https://doi.org/10.1016/J.GEOMORPH.2014.11.030

Hürlimann, M., Rickenmann, D., and Graf, C.: Field and monitoring data of debris-flow events in the Swiss Alps, Can. Geotech. J., 40, 161–175, 2003. https://doi.org/10.1139/t02-087

Iverson, R. M.: The physics of debris flows, Rev. Geophys., 35, 245–296, 1997. https://doi.org/10.1029/97RG00426

Johnson, C. G., Kokelaar, B. P., Iverson, R. M., Logan, M., Lahusen, R. G., and Gray, J. M. N. T.: Grain-size segregation and levee formation in geophysical mass flows, J. Geophys. Res. Earth Surface, 117, 2012. https://doi.org/10.1029/2011JF002185

Likos, W. J., and Lu, N.: Water vapor sorption behavior of smectite-kaolinite mixtures. Clays Clay Mineral, 50, 553–561, 2002. https://doi.org/10.1346/000986002320679297/METRICS

McArdell, B. W., Bartelt, P., and Kowalski, J.: Field observations of basal forces and fluid pore pressure in a debris flow, Geophys. Res. Lett., 34, 2007. https://doi.org/10.1029/2006GL029183

https://doi.org/10.5194/nhess-2023-126
Preprint. Discussion started: 14 September 2023

Natural Hazards and Earth System Sciences
Open Access
Discussions

McArdell, B. W., and Sartori, M.: The Illgraben torrent system. In E. Reynard (Ed.), World geomorphological landscapes, Landscapes and landforms of Switzerland (pp. 367-378), 2021. https://doi.org/10.1007/978-3-030-43203-4_25

Naef, D., Rickenmann, D., Rutschmann, P., and McArdell, B. W.: Comparison of flow resistance relations for debris flows using a one-dimensional finite element simulation model, Nat. Hazards Earth Sys. Sci., 6, 155–165, 2006. www.nat-hazards-earth-syst-sci.net/6/155/2006/

Pierson, T. C.:; Flow behavior of channelized debris flows, Mount St. Helens, Washington. In A. Abrahams (Ed.), Hillslope Processes (pp. 269–296), 1986.

Rickenmann, D.: Empirical Relationships for Debris Flows, Nat. Hazards, 19, 47–77, 1999.

Rietveld, H. M.: A profile refinement method for nuclear and magnetic structures, J. Applied Crystallography 2, 65–71, 1969. https://doi.org/10.1107/S0021889869006558

Salm, B.: Flow, flow transition and runout distances of flowing avalanches, Annal. Glaciol. 18, 221–226, 1993. https://doi.org/10.3189/S0260305500011551

Salm, B., Burkard, A., and Gubler, H. U.: Berechnung von Fliesslawinen. Eine Anleitung fuer Praktiker mit Beispielen, In Mitteilungen des Eidg. Institutes für Schnee- und Lawinenforschung (Vol. 47), 1990.

Schlunegger, F., Badoux, A., McArdell, B. W., Gwerder, C., Schnydrig, D., Rieke-Zapp, D., and Molnar, P.: Limits of sediment transfer in an alpine debris-flow catchment, Illgraben, Switzerland, Quat. Sci. Rev., 28, 1097–1105, 2009. https://doi.org/10.1016/j.quascirev.2008.10.025

Schürch, P., Densmore, A. L., Rosser, N. J., and McArdell, B. W.: Dynamic controls on erosion and deposition on debris-flow fans, Geology, 39, 827–830, 2011. https://doi.org/10.1130/G32103.1

Scotto Di Santolo, A., Pellegrino, A. M., and Evangelista, A.: Experimental study on the rheological behaviour of debris flow, Nat. Hazards Earth Sys. Sci., 10, 2507–2514, 2010. https://doi.org/10.5194/NHESS-10-2507-2010

Swisstopo: Bundesamt für Landestopografie, 2022. https://www.swisstopo.admin.ch/de/geodata.html

Uchida, T., Nishiguchi, Y., McArdell, B. W., and Satofuka, Y.: The role of the phase shift of fine particles on debris flow behavior: an numerical simulation for a debris flow in Illgraben, Switzerland, Can. Geotech. J., 58, 23-34, 2021. https://doi.org/10.1139/cgj-2019-0452

Voellmy, A.: Über die Zerstörungskraft von Lawinen, Schweiz. Bauzeitschrift, 73, 212–217, 1995. https://doi.org/10.5169/seals-61891

WSL. RAMMS::DEBRISFLOW User Manual v1.8.0 (v1.8.0). WSL, 2022. https://ramms.slf.ch/en/modules/debrisflow.html

https://doi.org/10.5194/nhess-2023-126
Preprint. Discussion started: 14 September 2023

Natural Hazards and Earth System Sciences
Discussions

Appendix A: measurements from monitoring station at the Illgraben

Event start	Front velocity CD 28-29 (m/s)	Max flow depth laser (m)	Max flow depth radar (m)	Mean bulk density laser (kg/m^3)	Peak velocity (quantile 0.99) laser CD 28-29 (m/s)	Peak velocity (quantile 0.99) radar CD 28-29 (m/s)	Peak discharge (quantile 0.99) laser CD 28-29 (m/s)	Volume laser CD 28-29 (m^3)	Flow duration (min)
21.06.2019 21:44	6.62	3.13	2.69	1870	6.55	6.57	147.61	97394	43
02.07.2019 01:26	3.86	1.75	1.73	1971	5.78	5.38	65.58	73188	52
26.07.2019 19:46	8.69	1.39	1.41	2223	9.74	9.98	93.26	113310	65
11.08.2019 19:07	6.95	1.81	1.89	2323	6.90	6.91	95.63	88064	88
20.08.2019 19:03	0.89	1.13	1.10	2031	1.36	1.36	8.06	6137	37
24.06.2021 17:11	8.18	2.40	2.49	1750	8.16	8.10	162.20	105032	38
06.07.2021 20:43	8.69	2.50	2.58	1605	8.65	8.67	186.61	76906	28
16.07.2021 05:43	2.78	2.38	2.44	1916	3.22	3.30	60.70	80879	77
07.08.2021 16:22	2.32	2.49	2.17	1884	2.89	2.74	41.19	38737	46
19.09.2021 08:57	1.25	1.13	1.22	1697	1.41	1.39	10.67	8538	43
05.06.2022 12:33	3.39	2.08	2.15	1690	4.14	4.32	55.42	39498	55
04.07.2022 22:54	8.18	2.49	2.60	1189	8.46	7.36	169.14	175929	39
08.09.2022 02:06	1.91	1.93	1.77	1592	1.85	1.87	20.94	9283	20

https://doi.org/10.5194/nhess-2023-126
Preprint. Discussion started: 14 September 2023

Natural Hazards and Earth System Sciences
Open Access
EGU
Discussions

Appendix B: Exemplary evaluation of the simulations of the debris flow event on the 24th of June 2021

Input data composed of raster and shape files, simulation settings and measurements from the monitoring station.

Event	24.06.2021
DTM	DTM_0.5.tif
DTM resolution [m]	0.5
calculation domain	calcdom.shp
release area	hydrograph.shp
stop parameter [%]	5
sim resolution [m]	0.5
end time [s]	600
dump step [s]	2
erosion layer	erosion.shp
erosion density [kg/m3]	2000
erosion rate [m/s]	0.025
pot. Erosion depth [per kPa]	0.1
critical shear stress [kPa]	1
max erosion depth [m]	1
density [kg/m3]	1750
inflow direction [°]	60
vol [m3]	105032
Qmax [m3/s]	162.2
t1 [s]	10
v [m/s]	8.18
Front velocity CD 28-29 (m/s)	8.18
Max flow depth laser (m)	2.4
Max flow depth radar (m)	2.49
Peak velocity (quantile 0.99) laser CD 28-29 (m/s)	8.16
Peak velocity (quantile 0.99) radar CD 28-29 (m/s)	8.1
Flow duration (min)	38
CD28-CD29	134m
CD27-CD29	460m
Froude number	1.69

Output data with velocity (v) and flow depth (av_maxd_P) as reference variables to determine the best-fit simulation (green) for each μ. The z-values are calculated for both, the laser and radar measurement. However, to determine the best fit simulations, only the laser value was considered, as it was deemed more reliable.

https://doi.org/10.5194/nhess-2023-126
Preprint. Discussion started: 14 September 2023

Natural Hazards and Earth System Sciences
Open Access
Discussions

Appendix C: Grain size data

Weight percent passing per mesh size for each sample.

Mesh size [mm]	21.06.2019	02.07.2019	26.07.2019	11.08.2019	20.08.2019	24.06.2021	06.07.2021	16.07.2021	07.08.2021	19.09.2021	04.10.2021	05.06.2022	04.07.2022	08.09.2022
16.0000	100.0	100.0	100.0	100.0	100.0	100.0	100.0	100.0	100.0	100.0	100.0	100.0	100.0	100.0
8.0000	85.0	99.8	88.3	86.5	87.2	91.8	86.2	80.6	85.3	89.0	88.1	86.4	81.7	84.4
4.0000	73.7	97.5	78.6	76.3	76.5	83.6	75.1	69.5	74.8	79.9	79.7	78.2	70.5	74.5
2.0000	66.0	92.5	71.0	68.5	69.0	76.7	68.0	63.1	68.6	73.5	73.7	71.5	63.2	68.1
1.0000	59.0	85.6	63.8	61.1	62.1	69.9	61.1	58.6	63.2	67.7	68.5	64.5	56.8	61.8
0.5000	52.0	77.6	56.7	53.8	55.3	62.5	53.7	54.4	57.6	60.9	62.6	56.6	50.2	54.9
0.2500	44.8	68.6	48.6	50.1	47.8	53.7	46.7	49.0	50.7	52.4	56.1	48.8	43.2	47.5
0.1250	37.6	59.0	41.3	44.0	40.6	44.9	39.1	42.1	43.4	43.6	47.8	41.5	35.8	40.4
0.0630	31.7	49.1	34.4	36.3	34.1	37.0	32.0	35.4	35.9	35.7	39.8	34.0	29.4	33.0
0.0462	28.3	44.4	30.5	32.6	30.7	33.2	28.7	32.2	32.3	32.1	36.0	29.8	26.3	29.3
0.0339	24.8	39.6	26.1	28.3	27.0	28.9	24.5	28.0	27.7	27.0	30.5	25.7	22.8	25.8
0.0224	19.4	30.8	20.1	21.5	20.6	22.9	18.9	22.1	21.7	20.4	23.6	19.9	17.3	20.4
0.0135	13.0	21.3	13.3	14.0	14.4	15.2	13.0	15.1	14.4	13.4	15.8	13.2	12.0	13.0
0.0081	7.9	12.5	8.0	8.4	8.9	8.9	7.1	9.5	8.6	8.0	9.5	8.3	7.1	7.9
0.0050	5.1	7.8	5.3	5.4	5.7	5.7	4.5	5.8	5.0	5.0	5.9	5.4	4.8	5.3
0.0032	3.2	4.8	3.5	3.6	3.7	3.8	3.1	4.1	3.4	3.2	4.0	3.8	3.5	3.9
0.0015	1.3	2.5	1.8	1.6	2.1	2.4	1.9	2.2	1.5	1.8	2.8	2.3	1.9	2.3
0.0000	0.0	0.0	0.0	0.0	0.0	0.0	0.0	0.0	0.0	0.0	0.0	0.0	0.0	0.0

https://doi.org/10.5194/nhess-2023-126
Preprint. Discussion started: 14 September 2023

Natural Hazards and Earth System Sciences
Open Access
Discussions

Appendix D: Results of powder x-ray diffraction analysis

Measured weight percent per mineral for all four analyzed samples.

	02.07.2019	26.07.2019	20.08.2019	16.07.2021
Albite	2.0	2.0	1.8	2.0
Calcite	10.6	7.4	10.2	17.9
Dolomite	24.4	16.7	23.7	19.4
Muscovite	17.7	22.2	19.6	18.2
Orthoclase	3.4	2.9	2.8	3.0
Quartz	29.9	36.0	29.2	30.9
Chlorite	0.3	0.1	0.2	0.0
Illite	11.3	12.1	11.7	8.4
Kaolinite	0.0	0.1	0.1	0.0
Smektite	0.2	0.6	0.7	0.3